

Effective Hamiltonian for nickelate oxides $\text{Nd}_{1-x}\text{Sr}_x\text{NiO}_2$

Hu Zhang,¹ Lipeng Jin,¹ Shanmin Wang,¹ Bin Xi,^{2,*} Xingqiang Shi,^{1,†} Fei Ye,¹ and Jia-Wei Mei^{1,‡}

¹*Shenzhen Institute for Quantum Science and Engineering, and Department of Physics, Southern University of Science and Technology, Shenzhen 518055, China*

²*College of Physics Science and Technology, Yangzhou University, Yangzhou 225002, China*

(Dated: December 3, 2019)

We derive the effective single-band Hamiltonian in the flat NiO_2 planes for nickelate compounds $\text{Nd}_{1-x}\text{Sr}_x\text{NiO}_2$. We first implement the first-principles calculation to study electronic structures of nickelates using the Heyd-Scuseria-Ernzerhof hybrid density functional and derive a three-band Hubbard model for Ni-O $pd\sigma$ bands of $\text{Ni}^+ 3d_{x^2-y^2}$ and $\text{O}^{2-} 2p_{x/y}$ orbitals in the NiO_2 planes. To obtain the effective one-band $t-t'-J$ model Hamiltonian, we perform the exact diagonalization of the three-band Hubbard model for the Ni_5O_{16} cluster and map the low-energy spectra onto the effective one-band models. We find that the undoped NiO_2 plane is a Hubbard Mott insulator, and the doped holes primarily locate on Ni sites. The physics of the NiO_2 plane is a doped Mott insulator, described by the one-band $t-t'-J$ model with $t = 265$ meV, $t' = -21$ meV and $J = 28.6$ meV. We also discuss the electronic structure for the “self-doping” effect and heavy fermion behavior of electron pockets of $\text{Nd}^{3+} 5d$ character in $\text{Nd}_{1-x}\text{Sr}_x\text{NiO}_2$.

I. INTRODUCTION

The layered high-temperature superconductors in copper oxides and iron pnictides have motivated the search for new superconductivity compounds with layered structures¹⁻⁴. Due to the similar crystal and electronic structure, LaNiO_2 has been theoretical studies as the possible analogs to the cuprates^{5,6}. Recently, the superconductivity with the critical temperature up to $T_c \sim 15$ K is indeed discovered in $\text{Nd}_{0.8}\text{Sr}_{0.2}\text{NiO}_2$ thin film⁷, albeit the presence of the superconductivity remains debated^{8,9}. Similar to copper oxides, perovskite nickelates (RNiO_3 , where R is rare earth or heavy metal such as Tl or Bi) display lots of strongly correlated physics properties, such as the sharp metal-insulator transitions, particular magnetic order, and charge order¹⁰⁻¹³. The reduced form of RNiO_3 leads to the infinite layered phase RNiO_2 ¹⁴⁻²⁰, which has a very flat NiO_2 plane of the square lattice for Ni^+ with one hole in the $d_{x^2-y^2}$ orbital. The superconductivity likely occurs in the NiO_2 plane with the charged carrier doping. In the cuprate superconductor compounds, the strong electronic interactions play a significant role in the electronic structure²¹, and the effective one-band Hamiltonian has been proposed to describe the low energy physics of the correlation effects for $3d^9$ electrons²¹⁻²³. To understand the strongly correlated electronic structures of the nickelate oxides $\text{Nd}_{1-x}\text{Sr}_x\text{NiO}_2$, we need to find out the proper effective (one-band) Hamiltonian to explore the similarity and difference from the cuprate compounds.

NdNiO_2 crystallizes in the $P4/mmm$ (No. 123) space group, as depicted in Fig. 1 (a). Four oxygens surround the nickel in a planar square environment (Fig. 1 (d)), and the crystal field splits the d orbitals as shown in Fig. 1 (e). Ni^+ has the d^9 electronic state configuration, and the highest partially occupied d orbital is $3d_{x^2-y^2}$. The rare-earth ion Nd^{3+} sits in the center of cuboid formed by eight oxygen ions as shown in Fig. 1 (c). As Nd^{3+} in Nd_2CuO_4 ²⁴ and Ho^{3+} in HoNiO_3 ²⁵, Nd^{3+} has the local $4f$ moment far below the Fermi energy level. $\text{Nd} 5d$ orbitals have the split energy levels, as shown in Fig. 1 (e), and near the Fermi energy, the lowest $5d$ orbital

in Nd^{3+} is d_{z^2} . Therefore, in the simple reckoning for the relevant electronic structure, there are 12 bands near Fermi energy level corresponding to mainly Ni d (5 states) and O p (2×3 states) and Nd d_{z^2} (1 state). Previous density functional theory (DFT) studies within the local density approximation (LDA) on LaNiO_2 ⁶ supports the rough impression of the non-magnetic electronic structures.

In this paper, we first implement the first-principles simulations to derive a three-band Hubbard model for Ni-O $pd\sigma$ bands of $\text{Ni}^+ 3d_{x^2-y^2}$ and $\text{O}^{2-} 2p_{x/y}$ orbitals in the NiO_2 planes. Based on the three-band Hubbard model, we perform the exact diagonalization for the Ni_5O_{16} cluster and obtain the low-energy one-band effective Hamiltonian for the NiO_2 planes. We also discuss the electronic structure for the “self-doping” effect and the heavy-fermion behavior of electron pockets of $\text{Nd}^{3+} 5d$ character in $\text{Nd}_{1-x}\text{Sr}_x\text{NiO}_2$. We present our main results in the two successive stages in Sec. II. We discuss the physics of the one-band $t - J$ model in the NiO_2 planes in Sec. III. In the Appendix, we present the results for $\text{La}_{1-x}\text{Sr}_x\text{NiO}_2$, implying the generic electronic structures of RNiO_2 series. We also include other supplementary results for $\text{Nd}_{1-x}\text{Sr}_x\text{NiO}_2$ in the Appendix.

The main results are summarized as follows. In Sec. II A, we first perform DFT calculations of $\text{Nd}_{1-x}\text{Sr}_x\text{NiO}_2$ within the Heyd-Scuseria-Ernzerhof (HSE) hybrid density functional. We notice that in the previous study of the nickelates RNiO_3 , the HSE hybrid functional method is essential to reproduce the experimentally observed magnetic ground state²⁶. On the generalized gradient approximation (GGA) level, DFT simulations suggest the G-type antiferromagnetic (AFM within the NiO_2 plane and AFM between NiO_2 planes along the c direction) ground state of the moment on Ni sites in the parent compound NdNiO_2 . The HSE results for $\text{Nd}_{1-x}\text{Sr}_x\text{NiO}_2$ adopt the G-type spin configuration to mimic strong spin correlations. In Sec. II B, we describe the electronic structures based on the DFT simulations. Three-dimensional electron Fermi pockets of Nd $5d$ character are found near Fermi energy and behave as a heavy-fermion system due to its coupling with the local moments of Nd $4f$, similar to the electron-doped cuprate $\text{Nd}_{1.8}\text{Ce}_{0.2}\text{CuO}_4$ ²⁷. We also

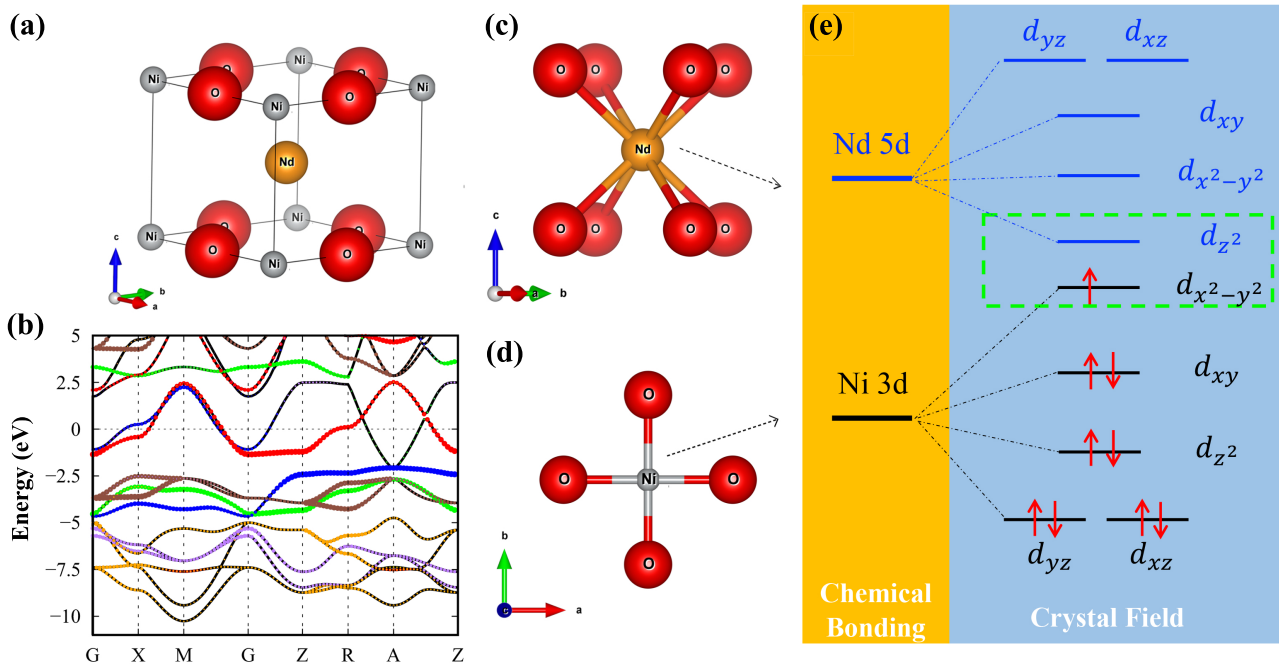


FIG. 1. (a) The crystal structure of NdNiO_2 with space group $P4/mmm$ (No. 123). (b) HSE06 band structures of the non-magnetic state in the parent compound NdNiO_2 along $\Gamma(0, 0, 0)$ - $X(0, 0.5, 0)$ - $M(0.5, 0.5, 0)$ - Γ - $Z(0, 0, 0.5)$ - $R(0, 0.5, 0.5)$ - $A(0.5, 0.5, 0.5)$ - Z directions. The projected band structures of d orbitals (red for $d_{x^2-y^2}$, blue for d_{z^2} , brown for $d_{xz/yz}$ and green for d_{xy}) in Ni and Nd, and $2p$ orbitals (orange for $p_{x/y}$ and purple for p_z) in O are also shown. The Fermi level is set at 0 eV. (c) Nd and its eight nearest neighbor O oxygens. (d) Ni and its four nearest neighbor O oxygens. (e) The crystal field splitting of Nd $5d$ and Ni $3d$ orbitals.

obtain the three-band Hubbard model for Ni-O $pd\sigma$ bands of $\text{Ni}^+ 3d_{x^2-y^2}$ and $\text{O}^{2-} 2p_{x/y}$ orbitals in the NiO_2 planes.

In Sec. II C, we derive the effective one-band Hamiltonian of the NiO_2 plane, following the standard procedure in the cuprates^{22,23}. We derive the parameters for the three-band Hubbard model of the Ni-O $pd\sigma$ bands for $\text{Ni}^+ 3d_{x^2-y^2}$ and $\text{O}^{2-} 2p_{x/y}$ orbitals from the LDA results from the first-principles simulations for the non-magnetic ground state for NdNiO_2 . Exact diagonalization (ED) studies of the Ni_5O_{16} cluster within the three-band Hubbard model are used to select and map the low-energy spectra onto the effective one-band t - t' - J model. According to ED results on finite clusters, in hole-doped nickelates, the doped holes primarily locate on Ni sites in a good agreement with the HSE results in Sec. II A and the experiment²⁸, while for cuprate the holes mainly locate on oxygen site^{22,23}. The physics of the NiO_2 is a doped Mott insulator described by the effective on-band t - t' - J model with $t = 265$ meV, $t' = -21$ meV, and $J = 28.6$ meV. The one-band effective Hubbard model is also given.

II. RESULTS

A. DFT results of $\text{Nd}_{1-x}\text{Sr}_x\text{NiO}_2$

We performed first-principles calculations based on DFT²⁹ with the HSE06 hybrid functional³⁰ as implemented in the Vienna Ab Initio Simulation Package (VASP)³¹⁻³³. We also implement PerdewBurkeErnzerhoff (PBE) functional in gen-

eralized gradient approximation (GGA)³⁴ and strongly constrained and appropriately normed semilocal density functional (SCAN) in meta-GGA³⁵ for comparisons. We use an energy cutoff of 500 eV and $12 \times 12 \times 12$, $4 \times 4 \times 4$, and $4 \times 4 \times 4$ Monkhorst-Pack grids³⁶ in the PBE, SCAN and HSE06 calculations, respectively. The $4f$ orbitals in Nd^{3+} are expected to display the local magnetic moment as Nd^{3+} in Nd_2CuO_4 ²⁴ and Ho^{3+} in HoNiO_3 ²⁵, and we treat them as the core-level electrons in the Nd pseudopotential in the HSE06 calculations. We check the results with $4f$ valence electrons pseudopotential within GGA+U ($U_{4f} = 10$ eV) scheme³⁷ in Appendix A. We also check that the spin-orbit coupling does not significantly change the DFT results in the Appendix. Therefore, we only present the simulations by taking $4f$ the core-level electrons in Nd pseudopotential and do not include the spin-orbit coupling in our HSE06 hybrid functional simulations.

We use the bulk lattice constants $a = b = 3.9208$ Å, $c = 3.281$ Å¹⁶ for $\text{Nd}_{1-x}\text{Sr}_x\text{NiO}_2$ and didn't optimize the crystal structure during the DFT simulations. In this setup, the NiO_2 plane remains flat in the doped case $\text{Nd}_{0.75}\text{Sr}_{0.25}\text{NiO}_2$. We didn't consider the lattice distortion effect upon doping in the doped nickelate oxides.

Figure. 1 (b) is the HSE06 band structure for the non-magnetic state in NdNiO_2 . The band ordering is different from the crystal field theory in Fig. 1 (e) due to the covalent effect in the hybridizations between d orbitals (Nd and Ni) and $2p$ orbitals (O). There are 12 electronic bands near the Fermi energy E_F , corresponding to orbitals mainly of Ni d (5 states)

and O p (2×3 states) and Nd d_{z^2} (1 state) for the relevant electronic structure. The O $2p$ bands extend from about -10 to -5 eV. The Ni $3d$ bands are distributed from -5 to 2 eV, while the broad Nd $5d$ states range from -1 to 10 eV. The Ni $3d_{x^2-y^2}$ and Nd $5d_{z^2}$ cross the Fermi energy E_F as expected from the crystal field splitting, as shown in Fig. 1 (e). Ni $3d_{x^2-y^2}$ is very broad along the Γ - X - M direction due to the strong $dp\sigma$ antibonding interaction with oxygen $p_{x/y}$ states and encloses holes centered at the M point. Ni $3d_{xy/xz/yz}$ bands localize near -4 eV due to the weak $dp\pi$ hybridization with O $2p$ states. Around A point, The Nd $5d_{z^2}$ state forms an electron pocket around the Γ point, goes up along Γ - Z direction, and lies above the Fermi energy level with $k_z = \pi/c$. The Nd $5d_{xy}$ lowers down and crosses the Fermi level, forming an electron pocket around A point.

Along Γ - Z direction, four O $2p_{x/y}$ bands and four Ni+ ($3dxz/yz$, $3d_{xy}$, and $3d_{x^2-y^2}$) bands have weak dispersions, indicating the two-dimensional features of these bands. Ni $3d_{z^2}$ and Nd $5d$ states are dispersive along with Γ - Z direc-

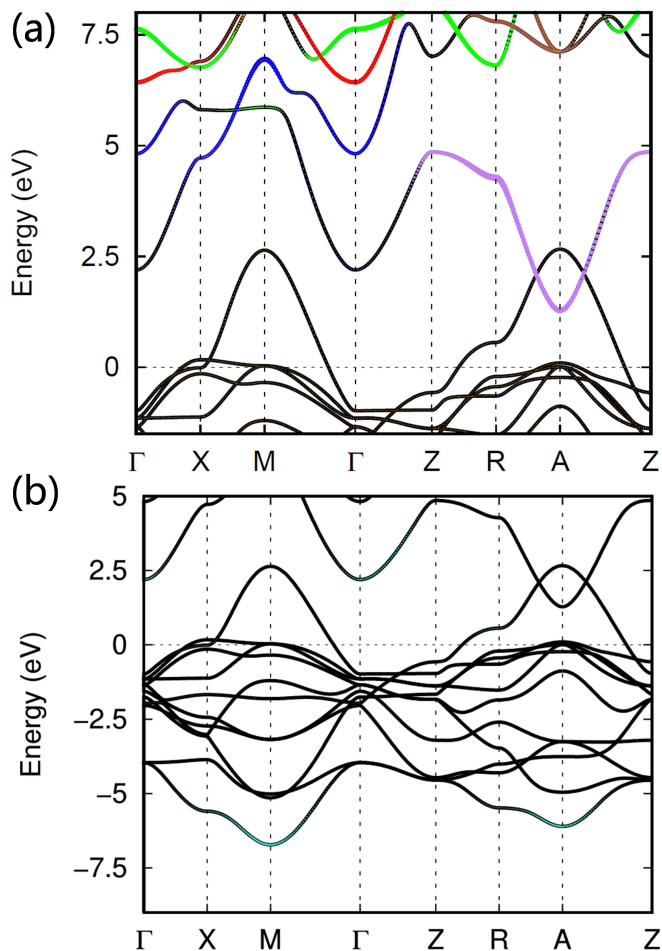


FIG. 2. GGA band structures of the non-magnetic state in the simulated SrNiO₂ in with the same structure as NdNiO₂. The projected band structures of d orbitals in Sr, and 4p orbitals in Ni are also shown. The color in (a) has the same meanings as Fig. 1 (b). The color turquoise in (b) indicates the projected Ni 4s orbital (mainly locates at Γ point at around 2.4 eV).

tions and three-dimensional extended. The two electron pockets around Γ and A points of the Nd $5d$ orbital character have the Ni orbitals mixing. However, such mixing is not quickly resolved in Fig. 1 (b) since the Nd $5d$ characters dominate the electron pockets and cover up the contributions from Ni orbitals. To further clarify the mixing character, we also present the band structure for the simulated SrNiO₂ in with the same structure as NdNiO₂, in order to eliminate Nd $5d$ orbitals in Fig. 2. From the comparing between Fig. 1 (b) and Fig. 2, we can see that Nd $5d_{z^2}$ band crosses E_F around Γ point with Ni $4s$ mixing, while Nd $5d_{xy}$ band crosses E_F around A point with Ni $4p_z$ mixing.

The GGA band structure of NdNiO₂ in Appendix A is quite similar to the LDA band structure of LaNiO₂⁶, indicating a generic electronic structure in the RNiO₂ family. Compared with the GGA band structure (Appendix A), for the non-magnetic state, the mixing of the exact exchange in the HSE06 hybrid functional separates the two bands crossing the Fermi energy E_F away from other bands, without significant change of dispersions and relative positions of the bands far from E_F . The separation of two bands can also be reproduced in the LDA+U results⁶. However, in the LDA+U scheme, Ni $3d_{z^2}$ is raised by U and crosses E_F when U is large⁶, different from the HSE06 hybrid functional simulation for the non-magnetic state.

The magnetization measurement and neutron powder diffraction didn't reveal the long-magnetic order in LaNiO₂ and NdNiO₂; however, the paramagnetic susceptibilities imply the (at least short) spin correlations^{15,16}. The absence of long-range magnetic order may be due to poor sample qualities, or due to the "self-doping" effects of the Nd $5d$ electron pockets. The strong correlation for electrons on Ni⁺ induce the magnetism in the system.

To demonstrate the correlation and magnetism in NdNiO₂, we calculate the magnetic moment and compare the ground state with the non-magnetic one within different functionals (GGA, SCAN, and HSE06). To save computation time, we consider the ferromagnetic spin configuration in the primary unit cell. The results are list in TABLE I. Than the non-magnetic state, the magnetic states have increased moments on Ni with increasingly lower ground state energies from GGA, SCAN to HSE06. For GGA, the magnetic state has even higher energy than the non-magnetic state, indicating the non-magnetic ground state within the GGA functional, consistent with the previous study in LaNiO₂⁶. The SCAN functional includes more correlation effects, and the magnetism is significantly enhanced. The magnetic ground state has further

TABLE I. Theoretical magnetic moments (in μ_B) on Ni in NdNiO₂ calculated with HSE06, SCAN, and PBE functional. ΔE is the energy difference between the non-magnetic state and the ferromagnetic state.

Functional	Magnetization	ΔE (meV)
HSE06	0.94	744.7
SCAN	0.76	142.7
GGA	0.05	-0.1

lower energy than the non-magnetic state in the HSE06 functional. The fact that the correlation achieves the magnetism is a strong indication that NdNiO₂ is magnetic if we include the correlations.

Even though there is no long-range magnetic order, we still impose static magnetic configurations on Ni ions in Nd_{1-x}Sr_xNiO₂ to mimic the spin correlations in the DFT simulations for electronic structures. We find the G-type AFM magnetic state has the lowest ground state energy within the GGA DFT simulations. Therefore, in the HSE06 simulations, we adopt the G-type AFM spin configurations on Ni using the $\sqrt{2} \times \sqrt{2} \times 2$ supercell to study the electronic structures of Nd_{1-x}Sr_xNiO₂ ($x = 0, 0.25$). Therefore, the Brillouin zone is folded by the G-type AFM spin configuration. However, without any confusion, we still use notations, Γ, X, M, Z, R, A , for high symmetry k-points in the folded Brillouin zone.

Figure. 3 displays the HSE06 band structures of Nd_{1-x}Sr_xNiO₂ ($x = 0, 0.25$) with G-type AFM magnetic configuration on Ni. In the HSE06 hybrid functional re-

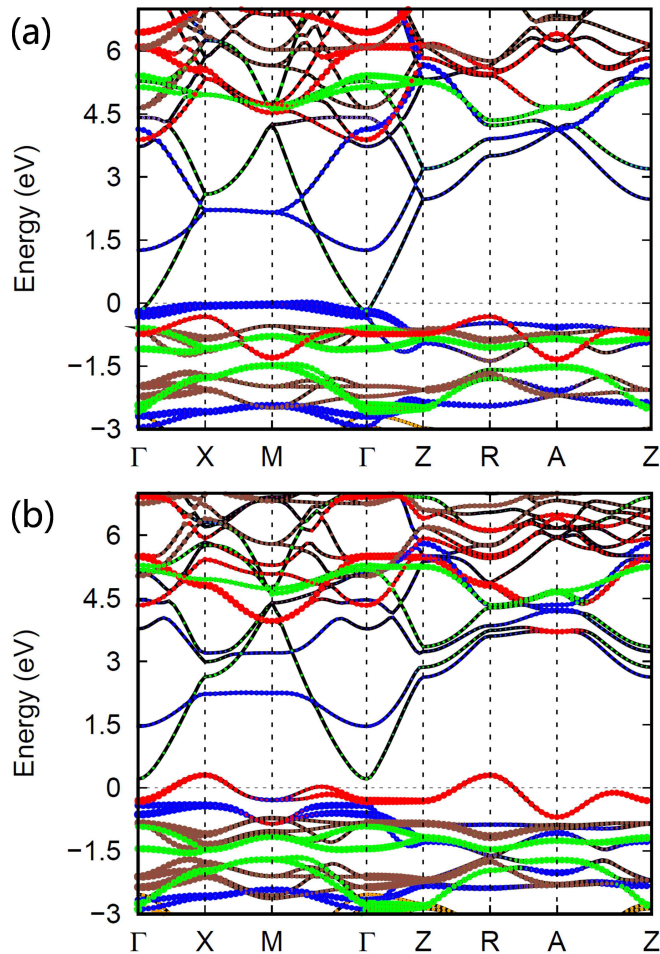


FIG. 3. HSE06 band structures of G-type AFM states for a $\sqrt{2} \times \sqrt{2} \times 2$ supercell in (a) NdNiO₂ and (b) Nd_{0.75}Sr_{0.25}NiO₂. The notations of Γ, X, M, Z, R and A are in the folded magnetic Brillouin zone. The color has the same meanings as Fig. 1 (b).

sults, the AFM magnetic configuration not only folds the band structure, but also dramatically change the bands near the Fermi energy E_F , very different from the GGA result for the G-type AFM magnetic configuration in the Appendix A. The significant change of band structures in the AFM states between GGA and HSE06 implies strong correlations in Nd_{1-x}Sr_xNiO₂.

In the G-type AFM state of NdNiO₂ (Fig. 3 (a)), the Nd $5d_{z^2}$ band is raised above the Fermi energy E_F by the correlation, eliminating the electron pocket of the Nd $5d_{z^2}$ character in the non-magnetic state (Fig. 1 (b)). The Nd $5d_{xy}$ band is also raised, but the electron pocket of this band still exists. We remind here again that the electron pocket of the Nd $5d_{xy}$ character has the Ni $4p_z$ orbital mixing. The Nd $5d_{xy}$ electron pocket locates around Γ point in the folded magnetic Brillouin zone. Therefore, the AFM spin correlation has an essential influence on the “self-doping” effect of Nd $5d$ electron pockets. For the Ni $3d$ band, the AFM correlation significantly renormalizes the bandwidth. The Ni $3d_{x^2-y^2}$ bands split into upper and lower Hubbard bands separated by around 5 eV due to the AFM spin configuration, indicating the strong correlation in NdNiO₂. The lower Hubbard $3d_{x^2-y^2}$ band locates lower than the Ni $3d_{z^2}$ band, bring the doping problem into a complicated situation.

When one Sr²⁺ ion substitutes Nd³⁺ in NdNiO₂, we dope an extra hole into the NiO₂ planes. To simulate the doped nickelate oxide, we calculate the band structures of Nd_{0.75}Sr_{0.25}NiO₂ (Nd₃SrNi₄O₈) in the $\sqrt{2} \times \sqrt{2} \times 2$ supercell with the G-type AFM spin configuration on Ni ions. Fig. 3 (b) is the HSE06 band structure of Nd_{0.75}Sr_{0.25}NiO₂. The Nd $5d_{xy}$ band goes up above the Fermi energy level, and the band minimum locates 0.2 eV. We can expect that Nd $5d_{xy}$ band contributes Hall coefficient at high temperatures at low dopings⁷. The doped hole does not go to the Ni $3d_{z^2}$ band. Instead, it locates on the $3d_{x^2-y^2}$ band, which goes up above $3d_{z^2}$ in Nd_{0.75}Sr_{0.25}NiO₂. Therefore, the doped hole does not polarize Ni²⁺ into the $S = 1$ local moment, but create an $S = 0$ hole-like doped charge carrier. The Ni $3d_{x^2-y^2}$ encloses the hole pockets around X point in the folded Brillouin zone (M in the original non-magnetic Brillouin zone). The HSE06 band structures in Fig. 3 suggest that the undoped NiO₂ plane is Hubbard-like Mott insulator, not the charge-transfer-like one as in the cuprate. The doped hole goes into Ni $3d_{x^2-y^2}$ orbital, creating an $S = 0$ hole-like charge carrier, rather than into the O²⁻ $2p_{x/y}$ orbitals.

B. Electronic structures of Nd_{1-x}Sr_xNiO₂

The presence of the electron pockets of Nd $5d$ bands suggests the “self-doping” effect, implying a small charge transfer from these pockets to the Ni-O sheets even without chemical doping. The “self-doping” effect also exists in the cuprate family, e.g., YBa₂Cu₃O₇ and Bi₂Sr₂CaCu₂O₈³⁸. The three-dimensional electron pockets of Nd $5d_{xy}$ states have the mixing with Ni $4p_z$ orbitals. The “self-doping” effect allows some charge transfer and changes the hole count in the NiO₂ planes, resulting in the metallic behavior even without chemical dop-

ing. In the Appendix A, we present the GGA band structure with the 4*f* valence electron pseudopotential within the GGA+U scheme. We can see that Nd 4*f* states have the mixing with Nd 5*d* states. Due to the presence of Nd 4*f* orbitals, the electron pockets of the Nd 5*d_{xy}* character hybridizes with the 4*f* local moments, behaving as a heavy-fermion system

$$H_K = \sum_{\mathbf{k}} \epsilon_{\mathbf{k}} a_{\mathbf{k}\sigma}^\dagger a_{\mathbf{k}\sigma} + J_K \sum_i \mathbf{s}_i \cdot \mathbf{S}_i^{4f}, \quad (1)$$

where $a_{\mathbf{k}\sigma}$ creates fermion with momentum \mathbf{k} on the electron pockets and \mathbf{s}_i and \mathbf{S}_i^{4f} are the spin operators for the 5*d* electrons and 4*f* local moments, respectively.

We now turn to the physics of the NiO₂ plane with the hole doping, following the process for the CuO₂ planes in cuprates^{22,23}. The HSE06 band structures in Fig. 3 suggest that the undoped NiO₂ plane is Hubbard-like Mott insulator, and the doped hole goes into Ni 3*d_{x²-y²}* orbital, creating an $S = 0$ hole-like charge carrier. Therefore, the physics of the NiO₂ plane with the charge doping is described by the three-band Hubbard model for the $dp\sigma$ bands of Ni 3*d_{x²-y²}* and O 2*p_{x/y}* orbitals. Fig. 4 schematically presents the orbitals of Ni 3*d_{x²-y²}* and O 2*p_{x/y}* with the green and brown colors corresponding to the positive and negative signs of wave functions, respectively.

We assume a vacuum state $d^{10}p^6$ and introduce the operators $d_{i\sigma}^\dagger$ and $p_{l\sigma}^\dagger$ creating the Ni 3*d_{x²-y²}* hole and the O 2*p_{x/y}* hole at the i -th Ni site and the l -th O site, respectively, with the spin $\sigma = \uparrow / \downarrow$. The holes hop between Ni 3*d_{x²-y²}* and O 2*p_{x/y}* orbitals with the amplitude t_{dp} , and among O 2*p_{x/y}* orbitals with the amplitude t_{pp} . We set the on-site potential of Ni 3*d_{x²-y²}* as $\epsilon_d = 0$, and the chemical potential difference

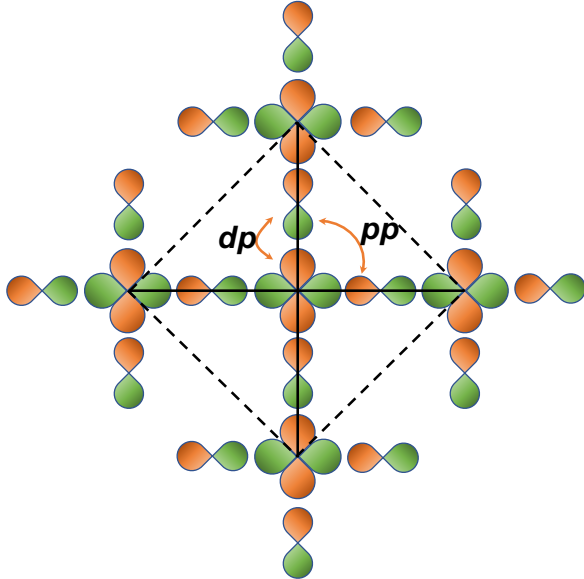


FIG. 4. Schematic representation of the orbitals (Ni 3*d_{x²-y²}* and O *p_{x/y}*) included in the three-band Hubbard model in the Ni₅O₁₆ cluster. The effective one-band model has the degree of freedom only on the five Ni 3*d_{x²-y²}* orbitals connected by the solid (t and J) and dashed (t' and J') lines.

between Ni 3*d_{x²-y²}* and O 2*p_{x/y}* orbitals as $\epsilon = \epsilon_p - \epsilon_d$. The strong correlations involve the on-site interactions U_p and U_d , and inter-site interactions U_{dp} and U_{pp} for holes on O 2*p_{x/y}* and Ni 3*d_{x²-y²}* orbitals. The three-band Hubbard model of the $dpsigma$ bands reads out

$$\begin{aligned} H_{dp} = & \sum_{\langle il \rangle \sigma} t_{dp} (d_{i\sigma}^\dagger p_{l\sigma} + \text{h.c.}) + \sum_{\langle ll' \rangle \sigma} t_{pp} (p_{l\sigma}^\dagger p_{l'\sigma} + \text{h.c.}) \\ & + \sum_{l\sigma} \epsilon p_{l\sigma}^\dagger p_{l\sigma} + U_d \sum_i n_{di\uparrow} n_{di\downarrow} + U_p \sum_l n_{l\uparrow} n_{l\downarrow} \\ & + \sum_{\langle il \rangle} U_{dp} n_{di} n_{pl} + \sum_{\langle ll' \rangle} U_{pp} n_{pl} n_{pl'}. \end{aligned} \quad (2)$$

Here $\langle \dots \rangle$ denotes the nearest neighbor bonds.

C. Effective t - t' - J model Hamiltonian of NiO₂ planes

The tight-binding parameters t_{dp} , t_{pp} , and ϵ can be obtained from the Wannier fitting^{39,40} of the 12 bands in the LDA simulations for the non-magnetic band structure of NdNiO₂. It is noteworthy that the HSE06 band structure in Fig. 1 (b) already contains the renormalization effect due to the strong correlations. There is double-counting for the correlations if we obtain the tight-binding parameters from the HSE06 band structure. The parameters are given as $\epsilon = 4.2$ eV, $t_{pd} = 1.3$ eV, $t_{pp} = 0.6$ eV. We choose a proper basis of the 3*d_{x²-y²}* and 2*p_{x/y}* for all positive t_{pd} and t_{pp} . To match the similar sizeable band splitting of the lower and upper Hubbard bands of the Ni 3*d_{x²-y²}* orbitals in the HSE06 band structure in Fig 3, we set the interaction terms as $U_d = 7.5$ eV, $U_p = 5.0$ eV, $U_{pd} = 4.0$ eV, and $U_{pp} = 2.0$ eV in the ED calculation for the derivation of the effective one-band Hamiltonian.

We follow the process in the cuprates^{22,23} to obtain the effective one-band Hamiltonian of the NiO₂ planes. We perform direct ED studies of the three-band Hubbard model H_{dp} in Eq. 2 and find the effective one-band Hamiltonian by the

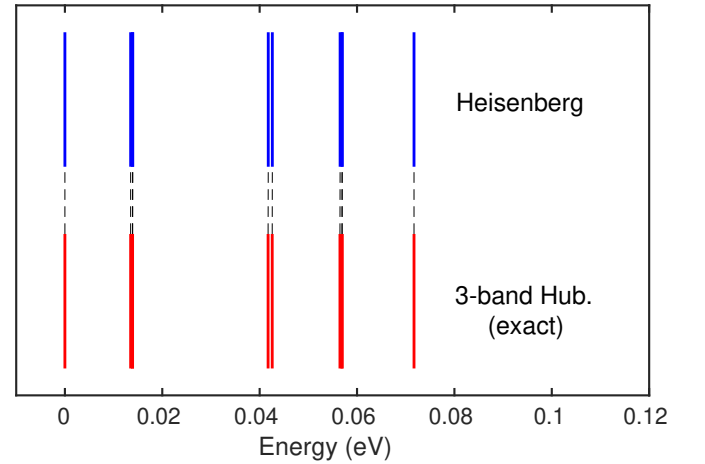


FIG. 5. The low-energy spectrum for Ni₅O₁₆ cluster calculated in the three-band Hubbard model in comparison to the mappings onto the Heisenberg Hamiltonian for the five-hole case.

low-energy spectrum mapping. We carry out the ED calculation for the Ni_5O_{16} cluster as shown in Fig. 4 with five and six holes for the undoped and hole-doped NiO_2 planes, respectively. The Ni_5O_{16} cluster is embedded in an array of $\text{Ni } 3d^9$ sites which shift the effective on-site energy of the outer O orbitals due to the inter-site Coulomb energy²³.

Figure 5 is the low-energy spectrum mapping for the Ni_5O_{16} cluster with five holes in the insulating ground state of the undoped NiO_2 planes. The spin-1/2 Heisenberg model

$$H_J = \sum_{ij} J_{ij} \mathbf{S}_i \cdot \mathbf{S}_j, \quad (3)$$

with the nearest neighbor and next nearest neighbor exchange interactions $J = 28.6$ meV and $J' = 0.4$ meV well reproduces the low-energy spectrum for the three-band Hubbard model as shown in Fig. 5. Therefore, we obtain the effective Heisenberg model for the undoped NiO_2 planes.

For the hole-doped phase, the calculated low-energy spectra for six holes in the Ni_5O_{16} cluster is shown in Fig 6. The chemical character of the hole in the ground state of the doped NiO_2 planes is Ni (76%) and O (24%) character, indicating that NdNiO_2 is in the regime of a Hubbard-Mott insulator, different from the cuprate where the doped holes primarily locate on O^{22,23}. The significant difference comes from a smaller U_d , but a larger $\epsilon = \epsilon_p - \epsilon_d$ in NdNiO_2 than those in La_2CuO_4 .

We map the three-band Hubbard model in Eq. (2) onto the single-band t - t' - J model

$$H_{tJ} = \sum_{ij\sigma} t_{ij} c_{i\sigma}^\dagger c_{j\sigma} + \sum_{ij} J_{ij} \mathbf{S}_i \cdot \mathbf{S}_j, \quad (4)$$

where $c_{i\sigma}$ is the electron operator on the Ni sites connected by the solid (t and J) and dashed (t' and J') lines in Fig. 4. We first fix $J = 28.6$ meV and $J' = 0.4$ meV as in the undoped case and then tune the hopping parameters t and t' . The suitable values for $t = 265$ meV, $t' = -21$ meV with the mapping spectra shown in Fig. 6. The signs for t, t' refer to hole notation. We notice that the low-energy spectra has the spectrum

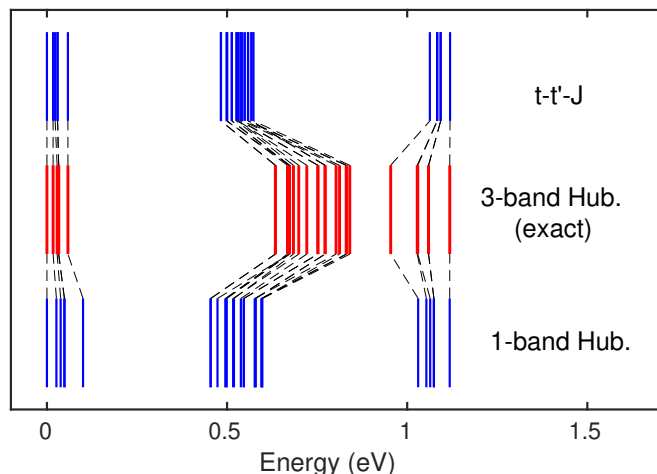


FIG. 6. The low-energy spectrum for Ni_5O_{16} cluster mapping onto effective one-band t - t' - J and Hubbard models.

width around 58 meV, approximately twice of the exchange strength $J = 28.6$ meV, in a good agreement with t - J model calculations for the cuprate, which show that, independent of the value of t , the dressing of the hole moving in the antiferromagnetic back-ground reduces the quasi-particle bandwidth to the twice of J ⁴¹.

We also map the low-energy spectra onto one-band Hubbard model

$$H_{1b} = \sum_{ij\sigma} t_{ij} c_{i\sigma}^\dagger c_{j\sigma} + U \sum_i n_{i\uparrow} n_{i\downarrow}, \quad (5)$$

with $t = 254$ meV, $t' = -30$ meV and $U = 6$ eV in Fig. 6. The one-band Hubbard model gives the similar charge-transfer gap as the three-band Hubbard model in the Ni_5O_{16} cluster.

III. DISCUSSIONS AND CONCLUSIONS

From the above derivation of the effective one-band $t - t' - J$ model Hamiltonian, we find that the physics of NiO_2 planes in $\text{Nd}_{1-x}\text{Sr}_x\text{NiO}_2$ is a doped Mott insulator, even further away from a conventional Fermi liquid than the superconducting cuprates. The undoped CuO_2 plane in the cuprate is a charge-transfer type Mott insulator, but the undoped NiO_2 plane in the nickelate is a Hubbard Mott insulator. Both the NiO_2 and CuO_2 planes have the same effective one-band t - t' - J model Hamiltonians, and they have the similar physics of the superconductivity.

The discovering of the superconductivity in the nickelate oxide⁷ certainly motivates the studies of the effective Hamiltonian in this paper. However, two recent experimental papers reported non-superconductivity results in $\text{Nd}_{1-x}\text{Sr}_x\text{NiO}_2$ ^{8,9}, getting the presence of superconductivity into controversy. The existence of the superconductivity in the doped nickelate oxides is a crucial issue and needs further exploring in the experiments. In this paper, our study is the consequence of a quantum-chemical description of $\text{Nd}_{1-x}\text{Sr}_x\text{NiO}_2$; however, we cannot provide direct theoretical implication of the existence of the superconductivity. The effective Hamiltonian in this work provides essential support for, and constraint on, models to describe the low-energy physics of the nickelate oxides, regardless of the presence of the superconductivity. In our recent experimental work⁴², we perform Raman scattering on NdNiO_2 single crystal and measure the Heisenberg superexchange strength $J = 25$ meV from the two-magnon peak, in a good agreement with our present work. Although the current situation is not clear, we hope that our work will help us understand the electronic structure of nickelate oxides.

In conclusion, we have explicitly derived a single-band effective t - t' - J model Hamiltonian for Ni-O based compounds starting from a three-band model based on the density functional theory.

Note added – At the stage of finishing the manuscript, we noticed related theoretical works for nickelates^{43–50}. The pairing of hole carriers in the oxygen $p\pi$ orbitals is discussed in Ref.⁴⁵. First-principles simulations within GGA have been worked out in Refs.^{43,44,47–50}. DMFT is carried out in Ref.⁵⁰,

and RPA analysis of the pairing symmetry is done in Ref.^{44,47}. The hopping parameters for the three-band Hubbard model are (implicitly or explicitly) given from the Wannier fitting in Refs.^{43,44,47-50}, with similar values to our work. The hopping parameters (t and t') of the effective Ni $3d_{x^2-y^2}$ band are also given in Refs.^{43,47-49} with $t \sim 370$ meV and $t' \sim -100$ meV, larger than the values $t = 265$ meV and $t' = -21$ meV renormalized by correlations in our work. The exchange interaction is estimated as $J = 100$ meV in Ref.⁴⁷, larger than our values $J = 28.6$ meV. The Hubbard-Mott scenario is also proposed in Ref.⁴⁶ and the charge-transfer gap is estimated $\epsilon = 7 \sim 9$ eV, larger than our value $\epsilon = 4.2$ eV. In the Ref.⁴⁶, the $S = 1$ Ni^{2+} state is proposed when the hole is doped into the NiO_2 planes, different from the $S = 0$ Ni^{2+} state in our work. We notice that if the charge-transfer gap is taken as the value we use in the work, $\epsilon = 4.2$ eV, the $S = 0$ Ni^{2+} state is favored according to the calculation in Ref.⁴⁶.

IV. ACKNOWLEDGEMENTS

J.W.M thanks J.S. Chen for the help of drawing Fig. 1. J.W.M was partially supported by the program for Guangdong Introducing Innovative and Entrepreneurial Teams (No. 2017ZT07C062). F.Y was supported by National Science Foundation of China (No. 11774143). The exact diagonalization is performed by $\mathcal{H}\Phi$ package⁵¹.

Appendix A: Supplementary DFT results for $\text{Nd}_{1-x}\text{Sr}_x\text{NiO}_2$

In this part, we provide the supplementary DFT results for $\text{Nd}_{1-x}\text{Sr}_x\text{NiO}_2$. The main purpose of the supplementary results is two-folded: (a) check the validity of the Nd pseudopotential with the core-level $4f$ electrons; (b) compare the GGA and SCAN band structures to the HSE06 results in the main text. The spin-orbital coupling is also checked in this section.

1. GGA+U calculations for the Nd $4f$ valence electron pseudopotential

As Nd^{3+} in Nd_2CuO_4 ²⁴ and Ho^{3+} in HoNiO_3 ²⁵, Nd^{3+} has the local $4f$ moment far below the Fermi energy level E_F . In the main text, we treat the $4f$ electrons in Nd^{3+} as the core-level electrons in the Nd pseudopotential. In this subsection, we verify the validity of this treatment.

Figure 7 are the band structure of G-type AFM states for NdNiO_2 and $\text{Nd}_{0.75}\text{Sr}_{0.25}\text{NiO}_2$ calculated with $4f$ valence electron pseudopotential within GGA+U scheme. Without the U term, the $4f$ electrons form very localized bands near the Fermi level. In the G-type AFM states, the local moments of $4f$ electrons are also AFM within the same Nd plane and between Nd planes along the c direction. We take the on-site interaction for $4f$ electrons $U_{4f} = 10$ eV in the GGA+U calculation which splits the $4f$ bands above and below the Fermi energy level E_F . During the calculations, we also include the spin-orbital couplings.

According to Fig. 7, we can see that the $4f$ electron states couple to Nd $5d$ bands, however, doesn't significantly change the band structures near the Fermi level. Thus we can treat $4f$ orbitals as the core-level electrons in the Nd pseudopotential.

2. GGA and SCAN band structures

In this subsection, we present the band structures for $\text{Nd}_{1-x}\text{Sr}_x\text{NiO}_2$ within GGA and SCAN functionals with/without spin-orbital couplings in Fig. 8 and Fig. 9, respectively. Again, once soc is taken into account, there is no significant change in the band structures. The main features of SCAN band structures are very close to those in HSE06 band structures.

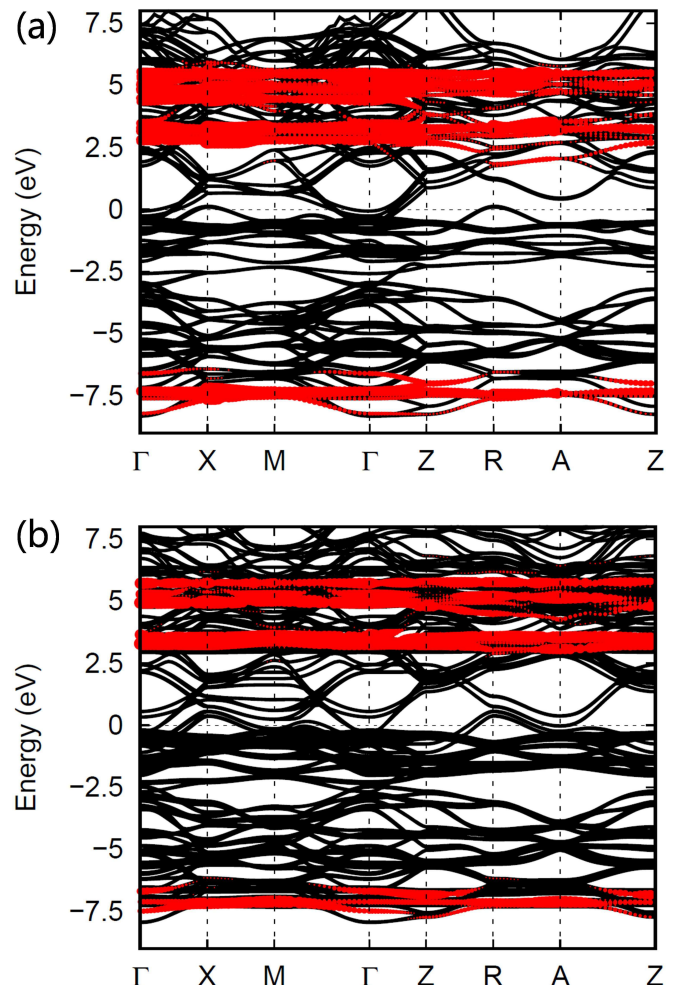


FIG. 7. GGA band structures of G-type AFM states for a supercell in (a) NdNiO_2 and (b) $\text{Nd}_{0.75}\text{Sr}_{0.25}\text{NiO}_2$ calculated with $4f$ valence electrons pseudopotential within GGA+U ($U_{4f} = 10$ eV) scheme with SOC. The notations of Γ , X, M, Z, R and A are in the folded magnetic Brillouin zone. The projected band structures of f orbitals (red) in Nd are also shown. The Fermi level is set at 0 eV.

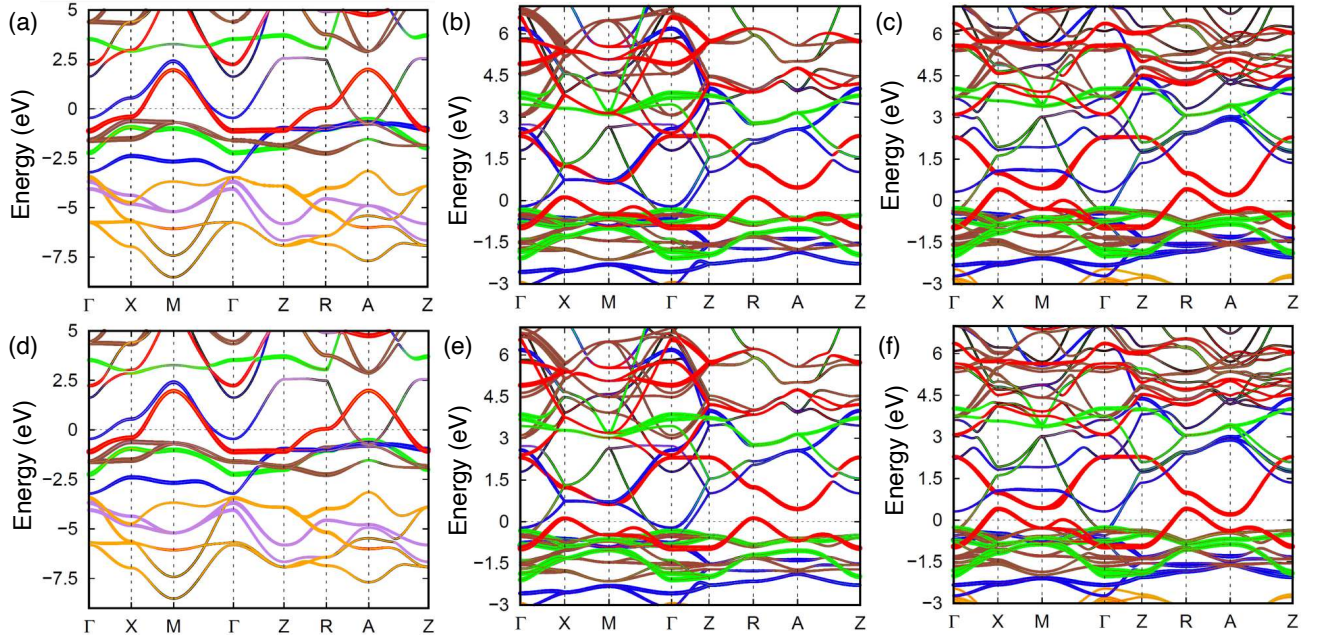


FIG. 8. GGA band structures of $\text{Nd}_{1-x}\text{Sr}_x\text{NiO}_2$. (a), (b), and (c) correspond to Fig. 1 (b) (the non-magnetic state for NdNiO_2), Fig. 3 (a) (the G-type AFM state for NdNiO_2) and (b) (the G-type AFM state for $\text{Nd}_{0.75}\text{Sr}_{0.25}\text{NiO}_2$), respectively, without SOC. (d), (e), and (f) are the results with turning on SOC.

Appendix B: HSE06 results of LaNiO_2

The LDA result for LaNiO_2 has been studied previously⁶. In this subsection, we implement the HSE06 hybrid functional to calculate band structures of the non-magnetic state in LaNiO_2 and G-type AFM states for a supercell in LaNiO_2 and $\text{La}_{0.75}\text{Sr}_{0.25}\text{NiO}_2$ in Fig. 10. The band structures are very similar to the results of NdNiO_2 , implying the generic electronic structures in the RNiO_2 family.

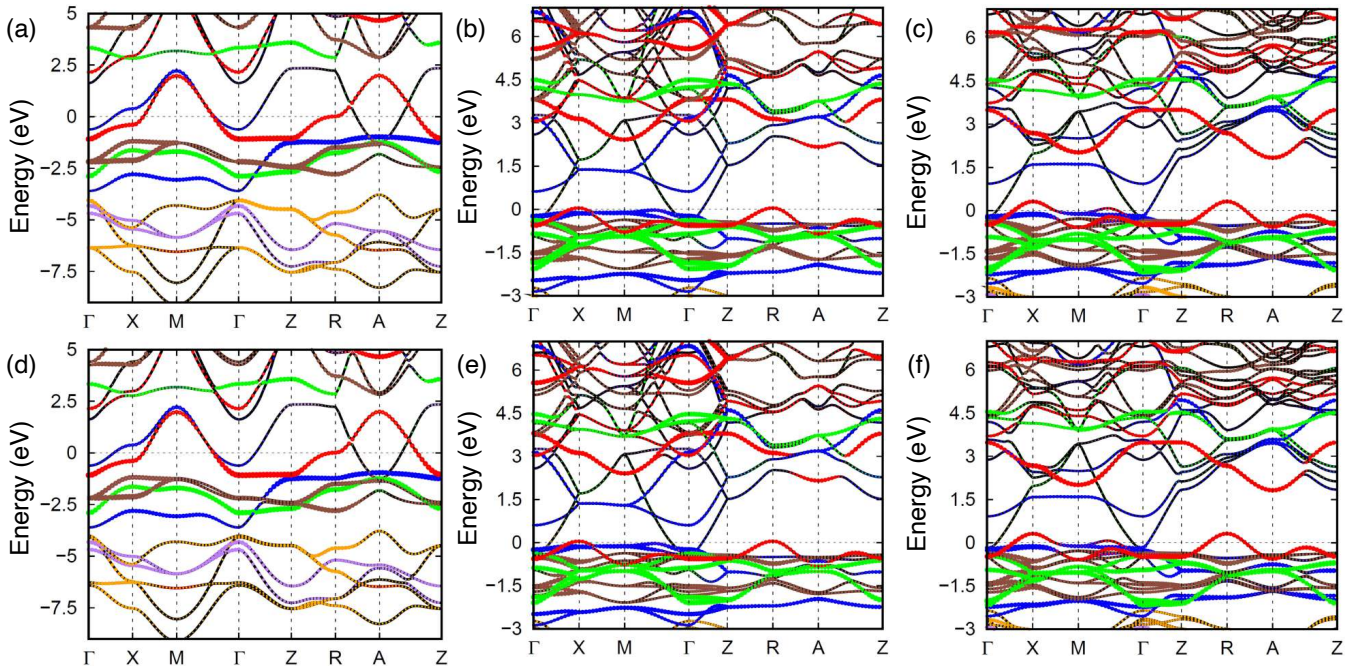


FIG. 9. SCAN band structures of $\text{Nd}_{1-x}\text{Sr}_x\text{NiO}_2$, similar to Fig. 8.

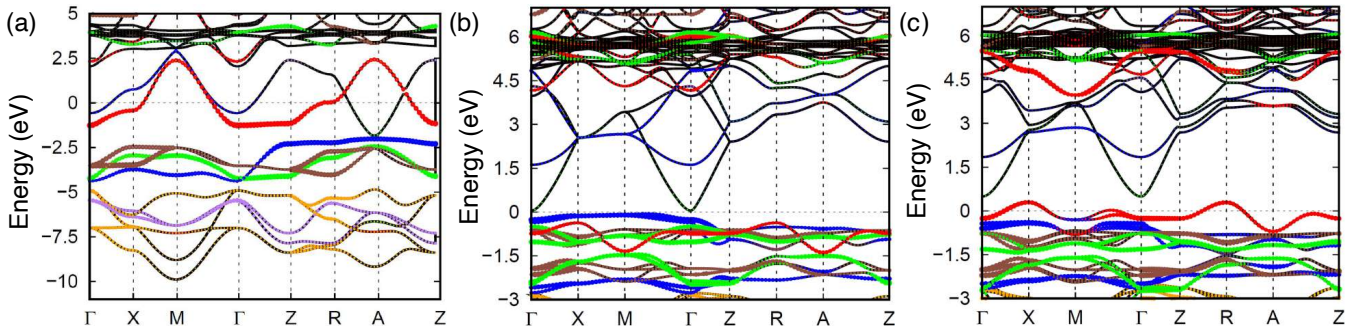


FIG. 10. HSE06 band structures of $\text{La}_{1-x}\text{Sr}_x\text{NiO}_2$ without SOC. (a) non-magnetic state for LaNiO_2 , (b) G-type AFM state for LaNiO_2 , and (c) G-type AFM state for $\text{La}_{0.75}\text{Sr}_{0.25}\text{NiO}_2$, corresponding to Fig. 1 (b), Fig. 3 (a) and (b), respectively.

* xibin@yzu.edu.cn

† shixq@sustech.edu.cn

‡ meijw@sustech.edu.cn

¹ J. G. Bednorz and K. A. Müller, “Possible high T_c superconductivity in the Ba-La-Cu-O system,” *Z. Physik B Condensed Matter* **64**, 189–193 (1986).

² Patrick A Lee, Naoto Nagaosa, and Xiao-Gang Wen, “Doping a Mott insulator: Physics of high-temperature superconductivity,” *Rev. Mod. Phys.* **78**, 17 (2006).

³ Yoichi Kamihara, Takumi Watanabe, Masahiro Hirano, and Hideo Hosono, “Iron-Based Layered Superconductor $\text{La}[\text{O}_{1-x}\text{F}_x]\text{FeAs}$ ($x = 0.05\text{--}0.12$) with $T_c = 26$ K,” *J. Am. Chem. Soc.* **130**, 3296–3297 (2008).

⁴ Hideo Hosono and Kazuhiko Kuroki, “Iron-based superconductors: Current status of materials and pairing mechanism,” *Physica C: Superconductivity and its Applications* **514**, 399 – 422 (2015), superconducting Materials: Conventional, Unconventional and Undetermined.

⁵ V. I. Anisimov, D. Bukhalov, and T. M. Rice, “Electronic structure of possible nickelate analogs to the cuprates,” *Phys. Rev. B* **59**, 7901–7906 (1999).

⁶ K.-W. Lee and W. E. Pickett, “Infinite-layer LaNiO_2 : Ni^{1+} is not Cu^{2+} ,” *Phys. Rev. B* **70**, 165109 (2004).

⁷ Danfeng Li, Kyuho Lee, Bai Yang Wang, Motoki Osada, Samuel Crossley, Hye Ryoung Lee, Yi Cui, Yasuyuki Hikita, and Harold Y. Hwang, “Superconductivity in an infinite-layer nickelate,” *Nature* **572**, 624–627 (2019).

- ⁸ Qing Li, Chengping He, Jin Si, Xiyu Zhu, Yue Zhang, and Hai-Hu Wen, "Absence of superconductivity in bulk $\text{Nd}_{1-x}\text{Sr}_x\text{NiO}_2$ ($x = 0.2, 0.4$)," arXiv e-prints, arXiv:1911.02420 (2019), [arXiv:1911.02420 \[cond-mat.supr-con\]](#).
- ⁹ Xiaorong Zhou, Zexin Feng, Peixin Qin, Han Yan, Shuai Hu, Huixin Guo, Xiaoning Wang, Haojiang Wu, Xin Zhang, Hongyu Chen, Xuepeng Qiu, and Zhiqi Liu, "Absence of superconductivity in $\text{Nd}_{0.8}\text{Sr}_{0.2}\text{NiO}_x$ thin films without chemical reduction," (2019), [arXiv:1911.04662 \[cond-mat.supr-con\]](#).
- ¹⁰ Maria Luisa Medarde, "Structural, magnetic and electronic properties of perovskites (R = rare earth)," *Journal of Physics: Condensed Matter* **9**, 1679–1707 (1997).
- ¹¹ G. Catalan, "Progress in perovskite nickelate research," *Phase Transitions* **81**, 729–749 (2008).
- ¹² S. Middey, J. Chakhalian, P. Mahadevan, J. W. Freeland, A. J. Millis, and D. D. Sarma, "Physics of ultrathin films and heterostructures of rare-earth nickelates," *Annu. Rev. Mater. Res.* **46**, 305–334 (2016).
- ¹³ S. Catalano, M. Gibert, J. Fowlie, J. Iiguez, J.-M. Triscone, and J. Kresisel, "Rare-earth nickelates RNiO_3 : thin films and heterostructures," *Reports on Progress in Physics* **81**, 046501 (2018).
- ¹⁴ Michel Crespín, Pierre Levitz, and Lucien Gatineau, "Reduced forms of LaNiO_3 perovskite. Part 1. – Evidence for new phases: $\text{La}_2\text{Ni}_2\text{O}_5$ and LaNiO_2 ," *J. Chem. Soc. Faraday Trans. II* **79**, 1181–1194 (1983).
- ¹⁵ M. A. Hayward, M. A. Green, M. J. Rosseinsky, and J. Sloan, "Sodium Hydride as a Powerful Reducing Agent for Topotactic Oxide Deintercalation: Synthesis and Characterization of the Nickel(I) Oxide LaNiO_2 ," *J. Am. Chem. Soc.* **121**, 8843–8854 (1999).
- ¹⁶ M. A. Hayward and M. J. Rosseinsky, "Synthesis of the infinite layer Ni(I) phase NdNiO_{2+x} by low temperature reduction of NdNiO_3 with sodium hydride," *Solid State Sciences* **5**, 839–850 (2003).
- ¹⁷ Masanori Kawai, Satoru Inoue, Masaichiro Mizumaki, Naomi Kawamura, Noriya Ichikawa, and Yuichi Shimakawa, "Reversible changes of epitaxial thin films from perovskite LaNiO_3 to infinite-layer structure LaNiO_2 ," *Appl. Phys. Lett.* **94**, 082102 (2009).
- ¹⁸ D. Kaneko, K. Yamagishi, A. Tsukada, T. Manabe, and M. Naito, "Synthesis of infinite-layer LaNiO_2 films by metal organic decomposition," *Physica C: Superconductivity* **469**, 936–939 (2009).
- ¹⁹ Masanori Kawai, Kazuya Matsumoto, Noriya Ichikawa, Masaichiro Mizumaki, Osami Sakata, Naomi Kawamura, Shigeru Kimura, and Yuichi Shimakawa, "Orientation Change of an Infinite-Layer Structure LaNiO_2 Epitaxial Thin Film by Annealing with CaH_2 ," *Crystal Growth & Design* **10**, 2044–2046 (2010).
- ²⁰ Ai Ikeda, Yoshiharu Krockenberger, Hiroshi Irie, Michio Naito, and Hideki Yamamoto, "Direct observation of infinite NiO_2 planes in LaNiO_2 films," *Applied Physics Express* **9**, 061101 (2016).
- ²¹ Philip W Anderson, "The Resonating Valence Bond State in La_2CuO_4 and Superconductivity," *Science* **235**, 1196–8 (1987).
- ²² F. C. Zhang and T. M. Rice, "Effective Hamiltonian for the superconducting Cu oxides," *Phys. Rev. B* **37**, 3759–3761 (1988).
- ²³ Mark S. Hybertsen, E. B. Stechel, M. Schluter, and D. R. Jennison, "Renormalization from density-functional theory to strong-coupling models for electronic states in Cu-O materials," *Phys. Rev. B* **41**, 11068–11072 (1990).
- ²⁴ H. Casalta, P. Bourges, M. d' Astuto, D. Petitgrand, and A. Ivanov, "Magnetic behavior of Nd in Nd_2CuO_4 above 1.5 K," *Phys. Rev. B* **57**, 471–475 (1998).
- ²⁵ M. T. Fernández-Díaz, J. A. Alonso, M. J. Martínez-Lope, M. T. Casais, and J. L. García-Muñoz, "Magnetic structure of the HoNiO_3 perovskite," *Phys. Rev. B* **64**, 144417 (2001).
- ²⁶ F. Y. Bruno, K. Z. Rushchanskii, S. Valencia, Y. Dumont, C. Carrétéro, E. Jacquet, R. Abrudan, S. Blügel, M. Ležaić, M. Bibes, and A. Barthélémy, "Rationalizing strain engineering effects in rare-earth nickelates," *Phys. Rev. B* **88**, 195108 (2013).
- ²⁷ P. Fulde, V. Zevin, and G. Zwicknagl, "Model for heavy-fermion behavior of $\text{Nd}_{1.8}\text{Ce}_{0.2}\text{CuO}_4$," *Zeitschrift für Physik B Condensed Matter* **92**, 133–135 (1993).
- ²⁸ M. Hepting, D. Li, C. J. Jia, H. Lu, E. Paris, Y. Tseng, X. Feng, M. Osada, E. Been, Y. Hikita, Y. D. Chuang, Z. Hussain, K. J. Zhou, A. Nag, M. Garcia-Fernandez, M. Rossi, H. Y. Huang, D. J. Huang, Z. X. Shen, T. Schmitt, H. Y. Hwang, B. Moritz, J. Zaanen, T. P. Devereaux, and W. S. Lee, "Electronic structure of the parent compound of superconducting infinite-layer nickelates," arXiv e-prints, arXiv:1909.02678 (2019), [arXiv:1909.02678 \[cond-mat.supr-con\]](#).
- ²⁹ R. O. Jones, "Density functional theory: Its origins, rise to prominence, and future," *Rev. Mod. Phys.* **87**, 897–923 (2015).
- ³⁰ Jochen Heyd, Gustavo E. Scuseria, and Matthias Ernzerhof, "Hybrid functionals based on a screened coulomb potential," *J. Chem. Phys.* **118**, 8207–8215 (2003).
- ³¹ G. Kresse and J. Furthmüller, "Efficient iterative schemes for ab initio total-energy calculations using a plane-wave basis set," *Phys. Rev. B* **54**, 11169–11186 (1996).
- ³² M. Gajdoš, K. Hummer, G. Kresse, J. Furthmüller, and F. Bechstedt, "Linear optical properties in the projector-augmented wave methodology," *Phys. Rev. B* **73**, 045112 (2006).
- ³³ J. Hafner, "Ab-initio simulations of materials using vasp: Density-functional theory and beyond," *J. Comput. Chem.* **29**, 2044–78 (2008).
- ³⁴ John P. Perdew, Kieron Burke, and Matthias Ernzerhof, "Generalized gradient approximation made simple," *Phys. Rev. Lett.* **77**, 3865–3868 (1996).
- ³⁵ Jianwei Sun, Adrienn Ruzsinszky, and John P. Perdew, "Strongly constrained and appropriately normed semilocal density functional," *Phys. Rev. Lett.* **115**, 036402 (2015).
- ³⁶ Hendrik J. Monkhorst and James D. Pack, "Special points for brillouin-zone integrations," *Phys. Rev. B* **13**, 5188–5192 (1976).
- ³⁷ A. I. Liechtenstein, Vi Vi Anisimov, and J. Zaanen, "Density-functional theory and strong interactions: Orbital ordering in mott-hubbard insulators," *Phys. Rev. B* **52**, R5467–R5470 (1995).
- ³⁸ Warren E. Pickett, "Electronic structure of the high-temperature oxide superconductors," *Rev. Mod. Phys.* **61**, 433–512 (1989).
- ³⁹ Arash A. Mostofi, Jonathan R. Yates, Young-Su Lee, Ivo Souza, David Vanderbilt, and Nicola Marzari, "wannier90: A tool for obtaining maximally-localised Wannier functions," *Comput. Phys. Commun.* **178**, 685–699 (2008).
- ⁴⁰ Arash A. Mostofi, Jonathan R. Yates, Giovanni Pizzi, Young-Su Lee, Ivo Souza, David Vanderbilt, and Nicola Marzari, "An updated version of wannier90: A tool for obtaining maximally-localised wannier functions," *Comput. Phys. Commun.* **185**, 2309–2310 (2014).
- ⁴¹ Elbio Dagotto, Alexander Nazarenko, and Massimo Boninsegni, "Flat quasiparticle dispersion in the 2d t-j model," *Phys. Rev. Lett.* **73**, 728–731 (1994).
- ⁴² Ying Fu, Le Wang, Hu Cheng, Shenghai Pei, Xuefeng Zhou, Jian Chen, Shaoheng Wang, Ran Zhao, Wenrui Jiang, Cai Liu, Mingyuan Huang, Xinwei Wang, Yusheng Zhao, Dapeng Yu, Shanmin Wang, and Jia-Wei Mei, "Electronic structures and spin fluctuations in nickelate oxide NdNiO_2 ," arXiv e-prints, arXiv:1911.03177 (2019), [arXiv:1911.03177 \[cond-mat.supr-con\]](#).

- ⁴³ Antia S. Botana and Michael R. Norman, “Similarities and differences between infinite-layer nickelates and cuprates and implications for superconductivity,” (2019), [arXiv:1908.10946 \[cond-mat.supr-con\]](#).
- ⁴⁴ Hirofumi Sakakibara, Hidetomo Usui, Katsuhiko Suzuki, Takao Kotani, Hideo Aoki, and Kazuhiko Kuroki, “Model construction and a possibility of cuprate-like pairing in a new d9 nickelate superconductor (Nd,Sr)NiO₂,” (2019), [arXiv:1909.00060 \[cond-mat.supr-con\]](#).
- ⁴⁵ J. E. Hirsch and F. Marsiglio, “Hole superconductivity in infinite-layer nickelates,” (2019), [arXiv:1909.00509 \[cond-mat.supr-con\]](#).
- ⁴⁶ Mi Jiang, Mona Berciu, and George A. Sawatzky, “Doped holes in NdNiO₂ and high- T_c cuprates show little similarity,” (2019), [arXiv:1909.02557 \[cond-mat.supr-con\]](#).
- ⁴⁷ Xianxin Wu, Domenico Di Sante, Tilman Schwemmer, Werner Hanke, Harold Y. Hwang, Srinivas Raghu, and Ronny Thomale, “Robust $d_{x^2-y^2}$ -wave superconductivity of infinite-layer nickelates,” (2019), [arXiv:1909.03015 \[cond-mat.supr-con\]](#).
- ⁴⁸ Yusuke Nomura, Motoaki Hirayama, Terumasa Tadano, Yoshihide Yoshimoto, Kazuma Nakamura, and Ryotaro Arita, “Formation of 2D single-component correlated electron system and band engineering in the nickelate superconductor NdNiO₂,” (2019), [arXiv:1909.03942 \[cond-mat.supr-con\]](#).
- ⁴⁹ Jiacheng Gao, Zhijun Wang, Chen Fang, and Hongming Weng, “Electronic structures and topological properties in nickelates $Ln_{n+1}Ni_nO_{2n+2}$,” (2019), [arXiv:1909.04657 \[cond-mat.mtrl-sci\]](#).
- ⁵⁰ Siheon Ryee, Hongkee Yoon, Taek Jung Kim, Min Yong Jeong, and Myung Joon Han, “Induced Magnetic Two-dimensionality by Hole Doping in Superconducting Nd_{1-x}Sr_xNiO₂,” (2019), [arXiv:1909.05824 \[cond-mat.supr-con\]](#).
- ⁵¹ Mitsuaki Kawamura, Kazuyoshi Yoshimi, Takahiro Misawa, Youhei Yamaji, Syngye Todo, and Naoki Kawashima, “Quantum lattice model solver $\mathcal{H}\phi$,” *Computer Physics Communications* **217**, 180–192 (2017).